Iron in the Sargasso Sea (Bermuda Atlantic Time-series Study region) during summer: Eolian imprint, spatiotemporal variability, and ecological implications

P. N. Sedwick,[1] T. M. Church,[2] A. R. Bowie,[3] C. M. Marsay,[1] S. J. Ussher,[4] K. M. Achilles,[2,5] P. J. Lethaby,[1,6] R. J. Johnson,[1] M. M. Sarin,[2] and D. J. McGillicuddy[7]

Received 31 December 2004; revised 13 July 2005; accepted 10 August 2005; published 13 October 2005.

[1] We report iron measurements for water column and aerosol samples collected in the Sargasso Sea during July-August 2003 (summer 2003) and April-May 2004 (spring 2004). Our data reveal a large seasonal change in the dissolved iron (dFe) concentration of surface waters in the Bermuda Atlantic Time-series Study region, from ~1–2 nM in summer 2003, when aerosol iron concentrations were high (mean 10 nmol m^{-3}), to ~0.1–0.2 nM in spring 2004, when aerosol iron concentrations were low (mean 0.64 nmol m^{-3}). During summer 2003, we observed an increase of ~0.6 nM in surface water dFe concentrations over 13 days, presumably due to eolian iron input; an estimate of total iron deposition over this same period suggests an effective solubility of 3–30% for aerosol iron. Our summer 2003 water column profiles show potentially growth-limiting dFe concentrations (0.02–0.19 nM) coinciding with a deep chlorophyll maximum at 100–150 m depth, where phytoplankton biomass is typically dominated by *Prochlorococcus* during late summer.

Citation: Sedwick, P. N., T. M. Church, A. R. Bowie, C. M. Marsay, S. J. Ussher, K. M. Achilles, P. J. Lethaby, R. J. Johnson, M. M. Sarin, and D. J. McGillicuddy (2005), Iron in the Sargasso Sea (Bermuda Atlantic Time-series Study region) during summer: Eolian imprint, spatiotemporal variability, and ecological implications, *Global Biogeochem. Cycles*, *19*, GB4006, doi:10.1029/2004GB002445.

1. Introduction

[2] The importance of iron in regulating marine primary production has been firmly established in the last 15 years [e.g., *Martin et al.*, 1990; *Coale et al.*, 1996; *Falkowski et al.*, 1998; *Boyd et al.*, 2000; *Jickells et al.*, 2005]. Mesoscale iron-fertilization experiments have shown that iron deficiency limits phytoplankton growth in the high-nitrate low-chlorophyll waters of the eastern equatorial Pacific, the subarctic Pacific and the Southern Ocean [*Martin et al.*, 1994; *Coale et al.*, 1996; *Boyd et al.*, 2004; *Tsuda et al.*, 2003; *Boyd et al.*, 2000; *Gervais et al.*, 2002; *Coale et al.*, 2004], and shipboard experiments have provided evidence of episodic iron limitation in several continental-shelf environments [*Martin et al.*, 1990; *Hutchins and Bruland*, 1998; *Fitzwater et al.*, 2000; *Sedwick et al.*, 2000; *Hutchins et al.*, 2002]. In addition, laboratory and field studies suggest that iron availability may limit the growth of cyanobacteria, such as *Trichodesmium*, *Synechococcus* and *Prochlorococcus*, in the oligotrophic open ocean [*Rueter*, 1988; *Behrenfeld and Kolber*, 1999; *Mann and Chisholm*, 2000; *Berman-Frank et al.*, 2001]. There is thus a clear need to include iron in both conceptual and numerical models of the marine ecosystem [*Doney et al.*, 2001]. At present, however, our poor understanding of the spatial and temporal distribution of iron in the ocean serves to limit the accuracy of such models [*Archer and Johnson*, 2000; *Fung et al.*, 2000; *J. K. Moore et al.*, 2002, 2004]. This largely reflects the difficulties involved in sampling and measuring the low concentrations of iron in open ocean waters [*Johnson et al.*, 1997; *Coale et al.*, 1999; *Johnson et al.*, 2002].

[3] The Sargasso Sea, in the western subtropical North Atlantic, is among the most heavily studied areas in the open ocean, with ongoing time series programs including Hydrostation S, the Bermuda Atlantic Time-series Study (BATS), the Oceanic Flux Program and the Bermuda Testbed Mooring [*Michaels and Knap*, 1996; *Steinberg et al.*, 2001; *Conte et al.*, 2001; *Dickey et al.*, 2001]. Despite the wealth of oceanographic and biogeochemical data collected from this area, there are surprisingly few reported measurements of iron in the Sargasso Sea. Surface waters in this region have been generally regarded as "iron replete," given the high eolian flux of soil dust that is carried over the Atlantic from North Africa during summer months [*J. K.*

[1]Bermuda Biological Station for Research, St. George's, Bermuda.
[2]University of Delaware, Newark, Delaware, USA.
[3]University of Tasmania, Hobart, Tasmania, Australia.
[4]University of Plymouth, Plymouth, UK.
[5]Now at University of California, Santa Cruz, Santa Cruz, California, USA.
[6]Now at University of Hawaii, Honolulu, Hawaii, USA.
[7]Woods Hole Oceanographic Institution, Woods Hole, Massachusetts, USA.

0886-6236/05/2004GB002445$12.00

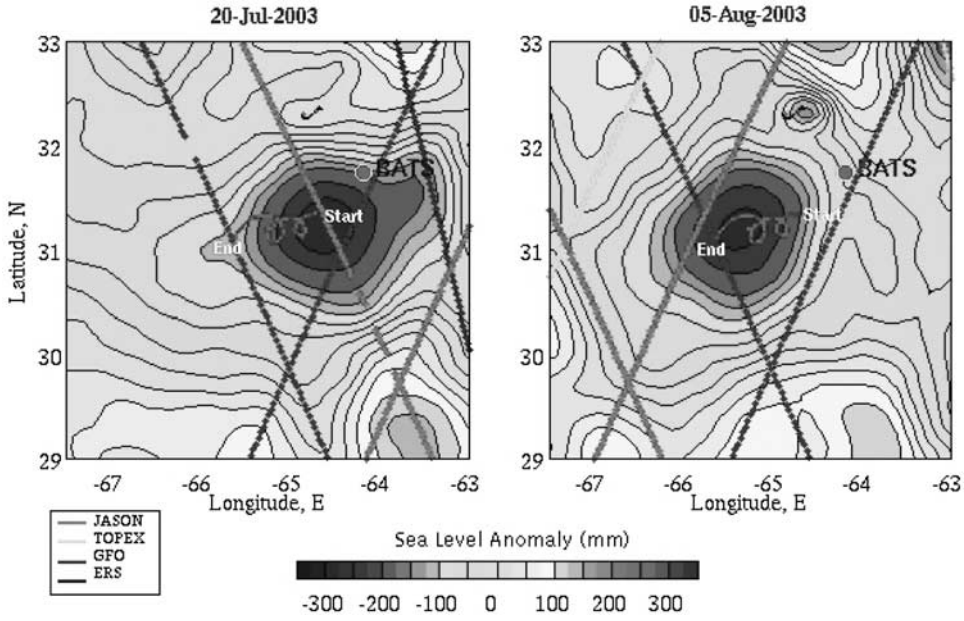

Figure 1. Objective analysis of sea level anomaly for (left) 20 July 2003 (just prior to summer 2003 cruise) and (right) 5 August 2003 (near end of summer 2003 cruise), showing location of target eddy (negative sea level anomaly shown in blue) and BATS site. The track of the drifting array during the cruise (red) is overlain on both panels, with initial (start) and final (end) points indicated. Real-time altimetric data were obtained from http://www-ccar.colorado.edu/~realtime/nwatlantic-real-time_ssh; altimeter ground tracks used in the analysis are identified in the legend. See color version of this figure at back of this issue.

Moore et al., 2002, 2004; *Prospero et al.*, 2002]. However, *Wu and Boyle* [2002] have recently presented iron data from two stations in the Sargasso Sea, from which they suggest that surface water dissolved iron concentrations may increase from relatively low values (~0.2 nM) during winter and spring to higher levels (~0.6 nM) in summer and fall, owing to the seasonal deposition of soil dust.

[4] Here we report water column and aerosol iron measurements for the BATS region, which we sampled over two weeks in July–August 2003 (summer 2003), during a period of high atmospheric dust loading, and over three days in April–May 2004 (spring 2004), when dust loadings were low. Our data provide new information concerning the temporal and spatial variability of iron in the Sargasso Sea, the effective solubility of aerosol iron in the subtropical North Atlantic, and the possible role of iron in regulating phytoplankton growth in subsurface waters of the subtropical gyres.

2. Methods

[5] Water column and aerosol samples for iron analysis were collected from the research vessel *Weatherbird II* during the periods 23 July to 6 August 2003 (summer 2003) and 29 April to 1 May 2004 (spring 2004).

2.1. Summer 2003 Cruise

[6] The summer 2003 cruise (22 July to 6 August 2003) coincided with calm weather, occasional scattered rain events, and high atmospheric loadings of soil dust, which was observed in aerosol and rain samples collected during the cruise, as well as in satellite images (e.g., see http://www.nrlmry.navy.mil/aerosol/). A major goal of our cruise was to examine the distribution of iron in the upper water column during a period of significant mineral aerosol deposition. Given the potential for lateral advection to confound observations of temporal changes in the vertical distribution of iron, we adopted a quasi-Lagrangian sampling strategy, and attempted to follow a single "parcel" of surface ocean water within a mesoscale eddy. A target cyclonic eddy was located to the southwest of the BATS site, using satellite altimetry measurements from the TOPEX/Poseidon, Jason, Geosat Follow-On, and European Remote Sensing platforms available through the Colorado Center for Astrodynamics Research Northwestern Atlantic Near Real-Time Altimeter Data Viewer [*Leben et al.*, 2002] (see http://www-ccar.colorado.edu/~realtime/nwatlantic-real-time_ssh). After a preliminary CTD survey on 22–23 July 2003, we deployed a free-floating sediment-trap array near the eddy center at 31°20′N, 64°41′W, with BATS-type particle interceptor traps at 150 m depth.

[7] Concurrent sea level anomaly analyses indicate that the floating array followed the core of the westward-moving eddy feature from 23 July to 6 August 2003, where it served as a reference point for our water column sampling (Figure 1). Both the initial (Figure 1, left) and final (Figure 1, right) positions of the drifting array lie within the eddy core, and the consistent looping trajectory indicates containment within the eddy. During this deployment, we carried out six trace-metal hydrocasts at stations

located ~1 km upwind of the drifting array. Five of these trace-metal hydrocasts were made to a depth of 1000 m, and were augmented by workboat sampling upwind of *Weatherbird II* for the clean collection of near-surface seawater (0–1 m and 10 m depth). Owing to rough weather, the sixth trace-metal hydrocast was limited to 100 m depth, with surface waters collected using a pole sampler (see below) from the ship's stern. We obtained daily CTD profiles adjacent to the drifting array, to provide a hydrographic context for our water column trace-metal sampling.

2.2. Spring 2004 Cruise

[8] The spring 2004 cruise (28 April to 1 May 2004) was carried out prior to any large seasonal inputs of North African soil dust, which typically occur between May and September [*Arimoto et al.*, 1995, 2003], although there had already been significant warming and shoaling of the surface mixed layer. For the purpose of comparison with data from the summer 2003 cruise, we again chose to sample the water column within a cyclonic eddy. As for the summer 2003 cruise, satellite altimetry allowed us to target a suitable cyclonic feature just east of the BATS site. On the basis of a preliminary CTD survey of this area, the eddy center was located near 31°25′N, 63°25′W, where we carried out trace-metal hydrocasts to 1000 m depth and CTD profiles on 29 and 30 April 2004. Seas were too rough to allow near-surface sampling from the workboat, so surface waters were collected from the ship's stern using a pole sampler (see below).

2.3. Sampling and Analysis

[9] Methods for the sampling and analysis of iron in the water column were similar to those detailed by *Sedwick et al.* [1997, 2000]. These methods were vetted during a recent intercomparison exercise as part of the international project Sampling and Analysis of Iron (SAFe), with results comparing favorably against those of other participating laboratories using a variety of analytical techniques for dissolved iron concentrations of ~0.1 nM and ~1 nM (K. S. Johnson et al., manuscript in preparation, 2005).

[10] All plastic ware used for sample collection, processing and analysis was rigorously acid cleaned following methods similar to those of *Sedwick et al.* [2000]. Water column samples were collected in modified 5 L Teflon-lined, external-closure Niskin-X samplers (General Oceanics Inc.) suspended from a Kevlar line, using plastic-coated end weights and solid PVC messengers. Surface water (0–1 m depth) samples were collected using a pole sampler, two 1-L wide-mouth low density polyethylene (LDPE, Nalgene) bottles secured in a Plexiglas frame at the end of a 5-m bamboo pole, which was extended from the work boat while underway, or from the ship's stern while slowly backing into the wind. Seawater samples were immediately filtered through acid-cleaned 0.4-μm pore size polycarbonate membranes, then acidified to pH 2.3 (0.52 mL Seastar Baseline quartz-distilled hydrochloric acid per liter of sample) in 125-mL Nalgene LDPE bottles, using trace-metal clean protocols in a shipboard Class-100 container laboratory.

[11] Dissolved iron (dFe) was determined in the 0.4-μm-filtered, acidified samples after >6 months storage, using flow injection analysis with in-line preconcentration and spectrophotometric detection modified after the method of *Measures et al.* [1995]. In addition, the same method was used to determine total-dissolvable iron (TDFe) in unfiltered samples that had been acidified to pH 1.7 (2 mL Seastar Baseline quartz-distilled hydrochloric acid per liter of sample) and stored for >6 months; TDFe thus provides a measure of dissolved iron plus particulate iron that is solubilized after extended storage at pH 1.7. The latter is assumed to include most of the particulate iron in seawater, with the exception of lattice-bound iron in refractory aluminosilicate particles.

[12] A rigorous estimate of the overall precision for the flow-analysis iron measurements is provided by multiple determinations, made on different days, of the Fe concentration in a single acidified seawater sample. For the method used in this study, overall precision has been estimated at ±7.4% (one relative standard deviation, n = 8) using a composite Southern Ocean seawater sample with a mean dissolved Fe concentration of 0.39 nM [*Bowie et al.*, 2004], and ±20.5% (1 relative standard deviation, n = 8) using a North Pacific surface seawater sample with a mean dissolved Fe concentration of 0.12 nM (P. N. Sedwick, unpublished data from SAFe intercomparison cruise, 2004). As described by *Bowie et al.* [2004], there are two components of the analytical blank for the flow-analysis method used in this study: (1) the so-called "zero-loading blank," which is an absorbance signal due to matrix differences between sample and flow stream; and (2) the acid reagent blank, which accounts for iron present in the hydrochloric acid added to samples. For the seawater analyses presented here, the zero-loading blank signal was equivalent to iron concentrations ranging from 0.074 to 0.25 nM for dFe and 0 to 0.37 nM for TDFe, and the acid reagent blank was determined to be 0.024 nM for dFe and 0.093 nM for TDFe. These blank values have been subtracted from the seawater Fe concentrations presented in this report. As described by *Bowie et al.* [2004], the detection limit for this flow-analysis method is estimated as the Fe concentration equivalent to a peak area that is three times the standard deviation on the zero-loading blank. On the basis of a typical peak-area reproducibility of ±5% for our samples of lowest concentration, we estimate detection limits below 0.04 nM for dFe and below 0.06 nM for TDFe.

[13] Aerosol samples were collected and processed for analysis of total iron using methods similar to those described by *Veron and Church* [1997]. Low-volume pumps (airflow ~2 m^3 h^{-1}) were used to pull air through acid-cleaned 47-mm-diameter Millipore HA (0.45 μm) filters mounted on a 7-m-high tower at the bow of the ship, while slowly steaming into the wind over extended periods (~12 hours). Filter halves were treated with a mixture of 48% hydrofluoric acid and 70% nitric acid, then, after complete dissolution of aerosol particles, any filter residue was removed and the solution was heated to dryness. The aerosol digestion residue was redissolved in 1 N nitric acid, and total iron was subsequently determined

by flameless atomic absorption spectrophotometry (Perkin Elmer 3300) using multielement calibration standards. The estimated analytical precision of this method is ±5%, based on repeated determinations. We assume that total iron determined in the digested aerosol material (as distinct from the total-dissolvable iron determined in seawater samples) accounts for all of the aerosol iron, including lattice-bound iron in aluminosilicate particles. Rainwater samples were collected using a polyethylene funnel and collection bottle, using a method similar to *Kim and Church* [2002]; these samples were immediately processed in the same manner as the water column samples, for later determination of iron by flow injection analysis.

[14] Subsamples of 0.4-μm-filtered seawater from the trace-metal hydrocasts were frozen in acid-cleaned LDPE bottles for the later analyses of macronutrients. Dissolved inorganic nitrate+nitrite and dissolved inorganic phosphate were determined using standard flow analysis methods at the Marine Science Institute Analytical Laboratory, University of California, Santa Barbara. The limits of detection for these analyses are around 0.05 μM for both nitrate+nitrite and phosphate.

3. Results and Discussion

[15] All data shown in Figure 2 represent water column measurements made or samples collected during daylight hours. Figures 2a, 2b and 2c show water column profiles of temperature (SeaBird SBE-911plus thermistor), salinity (SeaBird SBE-911plus conductivity sensor) and fluorescence (Chelsea Instruments fluorometer), respectively, from CTD deployments made immediately before or after the trace-metal hydrocasts during the summer 2003 cruise. Figure 2d shows concentration profiles of dissolved inorganic nitrate+nitrite and phosphate, and Figures 2e and 2f show dissolved iron (dFe) profiles from the summer 2003 and spring 2004 cruises, respectively. Figure 3 shows vertical concentration profiles of both dissolved iron (dFe) and total-dissolvable iron (TDFe), presented in chronological order, from the six trace-metal hydrocasts made during the summer 2003 cruise. Figure 4 shows total aerosol iron concentrations calculated from analyses of samples collected during the summer 2003 and spring 2004 cruises. The water column dFe, TDFe and macronutrient data, and calculated total aerosol iron concentrations, are provided as auxiliary electronic data supplements[1] to this paper.

3.1. Summer 2003

[16] The temperature (Figure 2a) and salinity (Figure 2b) profiles reveal a shallow surface mixed layer ranging from ~10 to 25 m in depth, overlying a seasonal thermocline extending to a depth of ~100 to 150 m. There was little vertical gradient in temperature and salinity between depths of ~150 m and 200 m, the relict mixed layer from the preceding winter-spring period, below which the permanent thermocline extended to a depth of ~1200 m. This water column structure is typical of the BATS region in late summer [e.g., *Steinberg et al.*, 2001]. The broad, well-defined fluorescence maximum centered at ~120 m depth (Figure 2c), near the top of the nitracline (Figure 2d), is also typical of the Sargasso Sea in late summer, when a deep chlorophyll maximum forms as nutrients are depleted from the upper euphotic zone [*Steinberg et al.*, 2001]. We observed relatively little change in the vertical structure of the water column adjacent to the drifting array over the period 23 July to 6 August, as evident from the six temperature and salinity profiles shown in Figure 2. This provides us with reasonable confidence in the success of our Lagrangian sampling strategy; that is, we assume that we sampled a single parcel of the upper ocean during the period of the summer 2003 cruise.

[17] Our summer 2003 dissolved iron profiles (Figure 2e) are remarkably consistent, with concentrations ranging over two orders of magnitude (0.02–2.0 nM dFe) in the upper water column. The general shape of these dFe profiles is qualitatively similar to the profile reported by *Bruland et al.* [1994] for a station in the central North Pacific subtropical gyre during summer. Pronounced near-surface maxima in dFe (0.89–2.0 nM, Figure 2e) and TDFe (1.8–4.7 nM, Figure 3) presumably reflect mineral aerosol input over the preceding summer months, when dust fluxes to the Sargasso Sea are highest [*Arimoto et al.*, 1995, 2003; *Jickells*, 1999] and eolian iron can accumulate in the shallow, oligotrophic surface mixed-layer [*Boyle et al.*, 1986, 2005; *Bruland et al.*, 1994; *Wu and Boyle*, 2002]. This interpretation is wholly consistent with our spring 2004 dFe profiles (Figure 2f), which display no near-surface enrichment (see section 3.2) during a period of relatively low aerosol iron loadings (<1 nmol m^{-3}, Figure 4). Satellite images reveal that our study region was impacted by a large North African dust plume during the summer 2003 cruise, and brown particles were clearly visible in aerosol and rainwater samples collected over the cruise period. Indeed, analysis of aerosol samples collected during the summer 2003 cruise (Figure 4) indicate high aerosol iron loadings, with an average concentration of 10 nmol m^{-3}.

[18] Below the surface mixed layer, surprisingly low dFe concentrations (0.02–0.19 nM) were measured in the 75–150 m depth range. The coincidence of these dissolved iron minima with the subsurface fluorescence maximum (Figures 2c and 2e) suggests removal of dissolved iron from the water column via particle scavenging and/or active uptake by phytoplankton [*Bruland et al.*, 1994; *Sedwick and DiTullio*, 1997; *Boyle et al.*, 2005]. Alternately, this dissolved iron minimum may have been a relict feature, reflecting low dissolved iron concentrations in the deeper mixed layer of the preceding winter-spring period, an explanation that is consistent with our spring 2004 iron data (see section 3.2 and Figure 2f). Subsurface minima also appear in our profiles of total-dissolvable iron (TDFe, Figure 3), which implies that both dissolved and particulate iron have been removed from the water column in the 75–150 m depth range; that is, vertical export of iron has occurred. Thus these subsurface iron minima do not simply reflect the repartitioning of iron between dissolved and suspended-particulate pools.

[1] Auxiliary material is available at ftp://ftp.agu.org/apend/gb/2004GB002445.

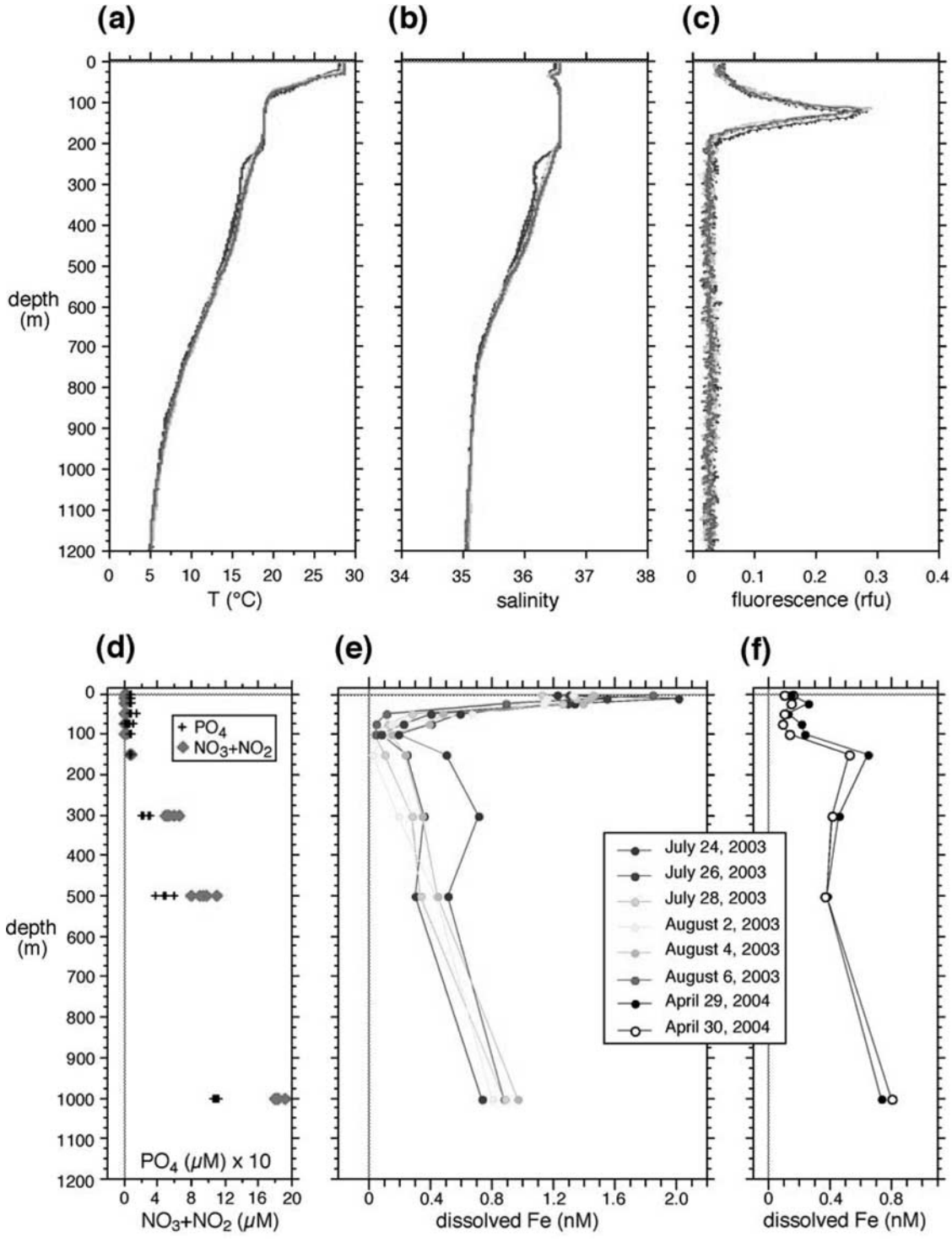

Figure 2. Water column profiles of (a) temperature, (b) salinity, (c) fluorescence, (d) dissolved nitrate+nitite ($NO_3 + NO_2$) and dissolved inorganic phosphate (PO_4), and (e) dissolved iron during the summer 2003 cruise; and (f) dissolved iron during the spring 2004 cruise. The color of data points in Figures 2a, 2b and 2c correspond to the legend in Figure 2e. See color version of this figure at back of this issue.

[19] Several of the summer dissolved iron profiles display a second concentration maximum at 300 m, while others show a gradual increase in concentration between 150 m and 500 m (Figure 2e). All of our dFe profiles show concentration increases with depth in the lower thermocline, from 0.30–0.51 nM dFe at 500 m depth to 0.73–0.97 nM dFe at 1000 m depth. The mean dissolved iron concentration at 1000 m is 0.85 ± 0.09 nM (n = 5), which is significantly

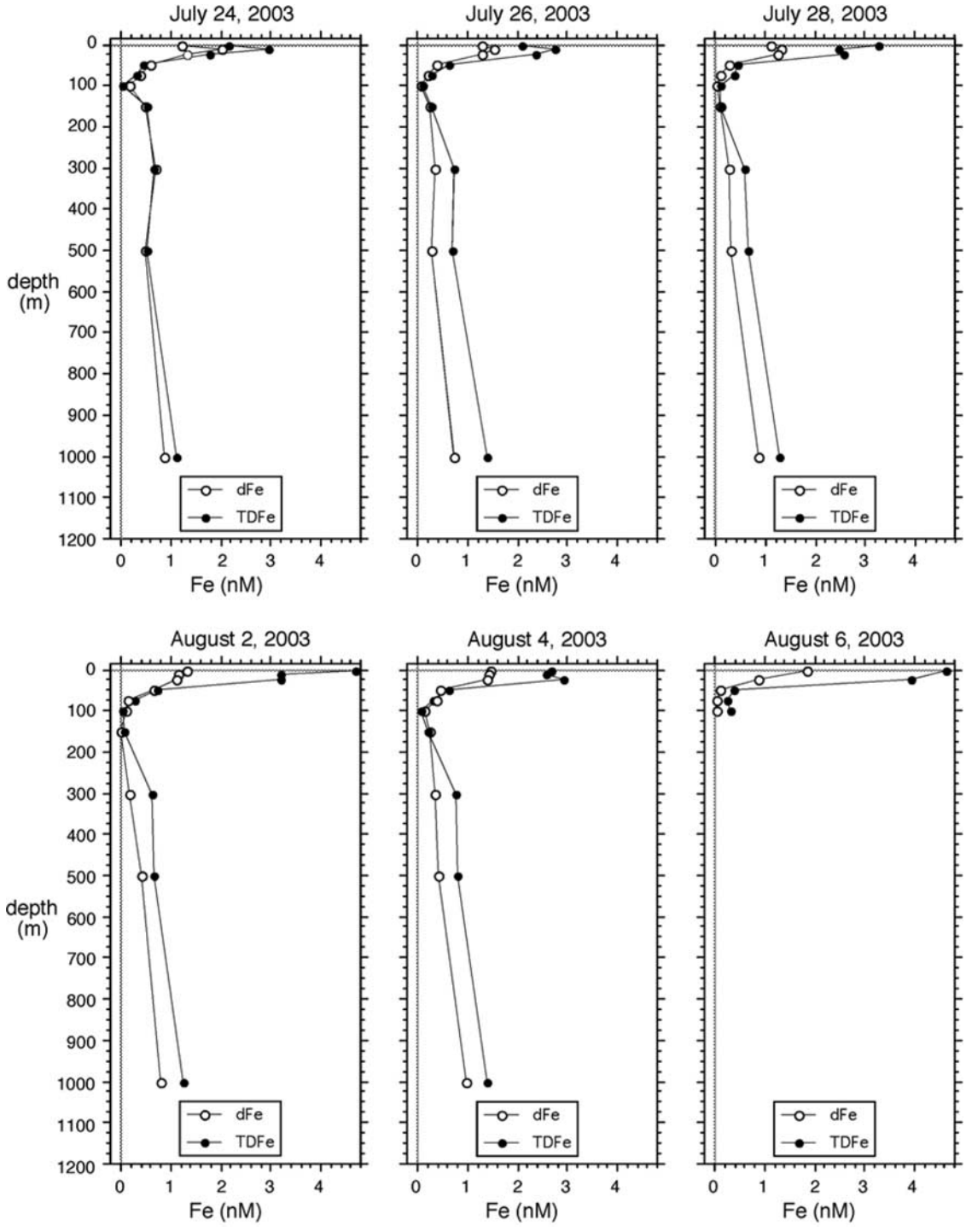

Figure 3. Time series of dissolved iron (dFe) and total-dissolvable iron (TDFe) water column profiles during the summer 2003 cruise.

higher than the value of ~0.65 nM reported by *Wu and Boyle* [2002] for a station near the BATS site in March 1998. However, a dissolved iron concentration of ~0.8 nM at 1000 m depth is reported by *Wu and Luther* [1996] for a station at the western edge of the Sargasso Sea [see *Bell et al.*, 2002, Figure 5]. Some of this discrepancy may reflect inter-method analytical differences: *Wu and Luther* [1996] used cathodic stripping voltammetry, *Wu and Boyle* [2002] used inductively-coupled plasma mass spectrometry (ICP-MS), and in this study we used flow-injection analysis. However, initial results from the SAFe intercomparison exercise suggest that there is little difference (<0.1 nM) between dissolved iron concentrations measured by our flow injection method and the ICP-MS method

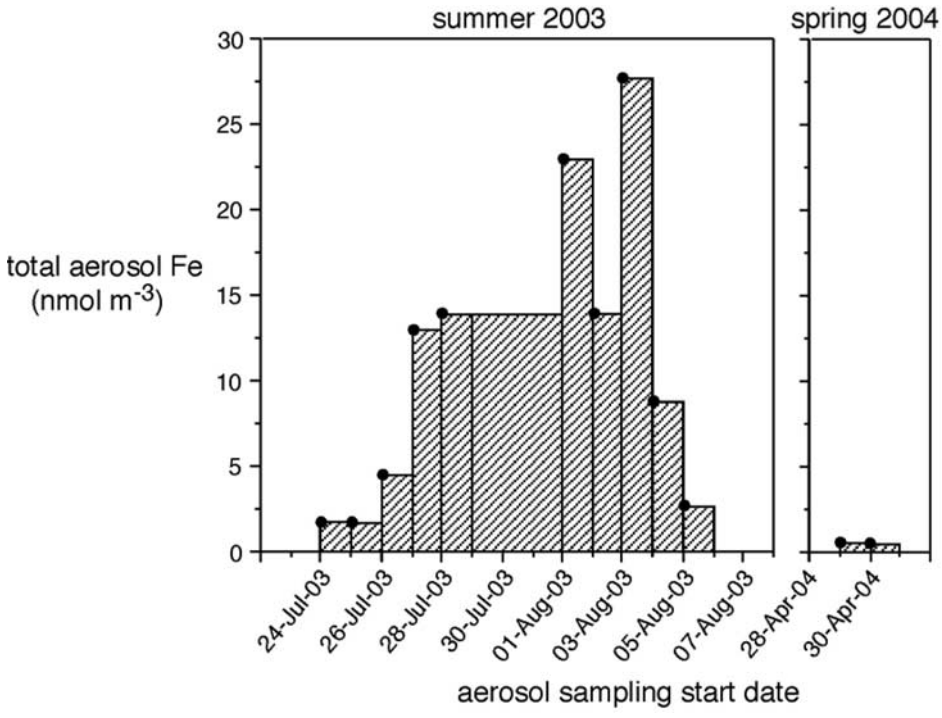

Figure 4. Total aerosol iron concentrations calculated from analysis of samples collected during (left) summer 2003 and (right) spring 2004 cruises. Data points are plotted with dates corresponding to the start of ~12-hour air sampling periods. For the summer 2003 cruise, dry deposition is calculated for the period 24 July to 6 August using aerosol Fe concentrations equal to the height of the shaded bars (note extrapolation of 28 July values to the period 29 July to 1 August, which was not sampled).

used by *Wu and Boyle* [2002] for North Pacific deep water (K. S. Johnson et al., manuscript in preparation, 2005). Our measured deep-water dFe concentrations of 0.73–0.97 nM are significantly higher than the 0.6-nM concentration maintained in the numerical models of *Archer and Johnson* [2000] and *Moore et al.* [2004], although our measured values can be reproduced by the parameterizations used in the recent iron-cycle model of *Parekh et al.* [2004].

3.2. Spring 2004

[20] Seasonal warming and stratification of the upper water column was well advanced at the time of our spring 2004 cruise. The CTD profiles from this cruise (data not shown) reveal a thermally-stratified upper water column capped by a surface mixed layer ~25 m deep, similar to that observed during the summer 2003 cruise. Surface water nitrate+nitrite concentrations were low (~0.1 μM), with the top of the nitracline located between 75 m and 100 m depth (data not shown). In contrast to the summer 2003 data, the spring 2004 profiles display no surface enrichment in dFe and TDFe, with uniformly low concentrations (0.09–0.26 nM dFe, 0.06–0.31 nM TDFe) over the upper 100 m of the water column (Figure 2f; TDFe data not shown). We surmise that the combined effects of deep convective mixing, biological uptake, particle scavenging and vertical export had removed dissolved iron from the upper water column during the preceding fall, winter and early spring [*Wu and Boyle*, 2002]. Satellite observations and aerosol transport models (see http://www.nrlmry.navy.mil/aerosol/) indicate no significant transport of soil dust to the BATS region in the months leading up to the spring 2004 cruise, and uniformly low aerosol iron concentrations of 0.54–0.74 nmol m^{-3} are estimated from analysis of total iron in our spring 2004 aerosol samples (Figure 4). Thus the dissolved iron profiles obtained in spring 2004 are likely to be representative of the BATS region before the major seasonal input of soil dust from North Africa. Our results from the summer 2003 and spring 2004 cruises are qualitatively consistent with the seasonal changes in iron distribution inferred by *Wu and Boyle* [2002]. However, the seasonal range in surface water dissolved iron concentrations that we have documented, from ~0.1 nM in spring to ~2 nM in late summer, is more than twice that reported by *Wu and Boyle* [2002] (~0.2–0.6 nM), and is significantly larger than the 0.3–0.7 nM range used in a recent model of iron cycling at the BATS site [*Weber et al.*, 2005].

[21] Below the euphotic zone, the spring 2004 iron data fall within the range of values observed in summer 2003, except at 150 m depth, where the spring 2004 profiles show dFe concentration maxima of 0.53–0.65 nM. This feature may reflect remineralization of iron-bearing particles exported from overlying surface waters during the spring "bloom" period in the BATS region [*Steinberg et al.*, 2001], and/or isopycnal advection, as has been suggested

for particulate organic carbon in our study area during spring [*Kim et al.*, 2003].

3.3. Temporal and Spatial Variability in Summer 2003

[22] For the summer 2003 data, there are no analytically-significant differences between the dFe profiles at water depths of 100, 500 and 1000 m (Figure 2e), although the vertical concentration trends discussed in sections 3.1 and 3.2 are robust. However, there are significant differences between the individual dFe profiles at water depths of 150 m and 300 m, and for all depths shallower than 100 m. With particle traps at 150 m depth tethered to surface floats, we assume that our drifting array followed the uppermost water column during the cruise period; that is, we expect our observations to be most Lagrangian above 150 m depth. This implies that differences in the dissolved iron profiles below ~150 m depth reflect spatial (lateral) variations in dissolved iron distribution. Indeed, the highest dFe concentrations at 150 m and 300 m depth are observed in the profile from 24 July (Figure 2e); corresponding temperature and salinity profiles (Figures 2a and 2b) show significant cold and fresh anomalies at ~250 m depth.

[23] For water depths shallower than 100 m, it is more difficult to ascribe inter-profile differences in iron concentrations to either spatial or temporal variability; more likely, our data reflect a combination of both lateral and temporal variations in iron distribution. Differences in the temperature and salinity profiles of the upper 100 m (Figures 2a and 2b), particularly for the 24 July profiles, suggest that we may have observed some small-scale lateral variations in the distribution of iron. However, the clear imprint of atmospheric deposition on the vertical distribution of iron implicates temporal variations in eolian input, given that our sampling coincided with the onset of high atmospheric dust loadings (Figure 4). Consistent with this interpretation, we observed a general increase in the iron concentrations of surface waters during the cruise period, with dFe increasing from 1.2 nM to 1.8 nM, and TDFe increasing from 2.2 nM to 4.7 nM (Figure 3). We note, however, that the surface water TDFe concentration on 4 August (2.7 nM) was significantly less than that on 2 August (4.6 nM) and 6 August (4.7 nM), suggesting some lateral variability in the distribution of particulate iron over distances on the order of kilometers.

[24] Such small-scale lateral variations in the surface water iron distribution could reflect wet deposition, which may be of comparable importance to dry deposition in delivering iron to the surface ocean [*Kim and Church*, 2001; *Gao et al.*, 2003; *Sarthou et al.*, 2003]. Wet deposition would be expected to result in patchy, episodic iron deposition during the summer months, when short-lived, isolated rain showers are common in the Bermuda region. We observed seven highly-localized rain events during the summer 2003 cruise, and collected rainwater samples that were visibly loaded with soil dust. Total-dissolvable iron concentrations in these rainwater samples range from 137 nM to as high as 12.3 μM (P. N. Sedwick, unpublished data, 2005).

[25] The temporal evolution of dFe and TDFe concentrations in the 10–25 m depth range is less clear. Our iron concentration profiles from 24 and 26 July (Figure 3) show subsurface maxima in dFe and TDFe at 10 m depth, in the middle to lower portion of the surface mixed layer. Given that dust-derived iron (dissolved and particulate) may have a residence time as short as days to weeks in surface waters of the North Atlantic [*Jickells*, 1999; *Sarthou et al.*, 2003; *Croot et al.*, 2004], we speculate that these transient maxima may reflect eolian iron deposition prior to the summer 2003 cruise period.

[26] The possibility of significant lateral variations in iron concentrations over scales of kilometers to tens of kilometers must be given serious consideration in the context of Eulerian time series observations of the ocean, such as the BATS and Hawaii Ocean Time-series programs. For observations collected at a fixed site or group of sites, it will be difficult to distinguish between temporal and spatial variability. Such spatial variations, as well as temporal changes due to episodic eolian inputs, must also be considered in high-resolution numerical models. We note that our observations, made within cyclonic eddies, may not be representative of the "mean" vertical distribution of iron in the Sargasso Sea. Given the strong vertical gradients in iron described here, it is possible that isopycnal displacements associated with eddies could generate significant mesoscale structure in the iron distribution. Additional field observations are required to obtain a sufficiently synoptic iron distribution and a demonstrably reliable mean iron profile for the BATS region.

3.4. Implications for Aerosol Iron Solubility

[27] Our CTD profiles from the summer 2003 cruise (Figure 2) show strong density stratification in the upper 100 m of the water column, with only minor changes in the temperature and salinity profiles over the 14-day sampling period. This would suggest that the vertical redistribution of iron due to turbulent diffusion, convective mixing and/or wind shear was negligible, except within the shallow upper mixed layer. We can then use the observed increases in surface dFe and TDFe concentrations during the summer 2003 cruise to infer the effective solubility of aerosol iron added to the surface mixed layer over that period, assuming (1) no loss of iron from the surface mixed layer, and (2) no scavenging or biological uptake of dissolved iron. The measured concentration increases of ~0.6 nM dFe and ~2.5 nM TDFe between 24 July and 6 August (Figure 3) imply that the added aerosol iron has a solubility (= dFe increase/TDFe increase) of around 24%. It should be noted, however, that this estimate represents a likely upper limit, because TDFe does not include all of the particulate iron in the water column (see section 2.3), and because larger aerosol particles may have settled out of the surface mixed layer soon after deposition.

[28] Another way to estimate the effective solubility of aerosol iron is to compare the increase in the dFe inventory of the surface mixed layer with the total eolian iron deposition over the summer 2003 cruise period. For this calculation we assume that the eolian iron flux was dominated by dry deposition, since only isolated rain showers were observed during the cruise period, and that scavenging and biological uptake of dissolved iron was negligible. We

use the height of the shaded bars in Figure 4 to approximate the time-variation of aerosol iron concentrations over the period 24 July to 6 August 2003 (aerosol concentrations for 29 July to 1 August, when no samples were collected, are extrapolated from the 28 July value). Total dry deposition of iron is estimated from the product of the area of these bars (1.3×10^7 nmol m^{-3} s) and the deposition velocity of the mineral aerosol particles, for which we use a range of 0.3–3 cm s^{-1} assuming a modal size of 1–10 μm [*Arimoto et al.*, 2003; *Maring et al.*, 2003; *Reid et al.*, 2003]. This yields a total dry deposition of 4–40 μmol Fe m^{-2} over the 13-day period ending on 6 August, which equates to an addition of 2–20 nM of total iron over a surface mixed layer of 20 m depth. Notably, this estimate is consistent with the ~2.5 nM increase in the TDFe concentration of surface water samples collected during the cruise. If the ~0.6-nM increase in surface dFe concentrations is representative of the dissolved iron added to the surface mixed layer, an assumption that is not inconsistent with the data shown in Figure 3, then we arrive at an effective solubility of 3–30% for the aerosol iron.

[29] This estimated solubility range is at the high end of estimates derived from dissolution experiments using North Atlantic aerosols [*Zhu et al.*, 1997; *Chen and Siefert*, 2004; *Hand et al.*, 2004; *Baker et al.*, 2005], and is higher than the 1–2% solubility that has been prescribed in recent global-scale biogeochemical models [*Aumont et al.*, 2003; *Moore et al.*, 2004; *Parekh et al.*, 2004]. We note, however, that *Boyle et al.* [2005] have recently estimated a solubility of 30–40% for aerosol iron in the subtropical North Pacific, based on repeated measurements of iron in surface waters at the Hawaii Ocean Time-series site.

3.5. Implications for Phytoplankton Ecology

[30] The coincidence of an iron concentration minimum with the deep chlorophyll maximum (DCM) during the summer 2003 cruise may have important implications for phytoplankton ecology in the Sargasso Sea. Our results suggest that phytoplankton growing at the depth of the DCM must contend with low iron availability. The minimum dissolved iron concentrations (0.02–0.19 nM) at 100–150 m depth are comparable to surface waters in the eastern equatorial Pacific and the Southern Ocean, where phytoplankton community growth rates are known to be limited by iron deficiency [*Martin et al.*, 1990; *Gordon et al.*, 1997; *Coale et al.*, 2004].

[31] During late summer in the BATS region, algal biomass in the DCM is typically dominated by the prolific cyanobacterium *Prochlorococcus* [*Olson et al.*, 1990; *DuRand et al.*, 2001; *Steinberg et al.*, 2001]. Within the DCM, *Prochlorococcus* ecotypes are believed to maintain a competitive advantage over other phytoplankton through their ability to grow under conditions of very low irradiance [*Ting et al.*, 2002; *Rocap et al.*, 2003]. Our geochemical data imply that adaptation to very low iron availability, in addition to low-light adaptation, may allow these *Prochlorococcus* ecotypes to exploit this niche in the lower euphotic zone, where the growth of other phytoplankton is co-limited by availability of iron and light [*Sunda and Huntsman*, 1997]. This idea is consistent with the proposed evolution of *Prochlorococcus* under iron-deficient conditions [*Ting et al.*, 2002], and with the identification of several genes in the *Prochlorococcus* genome that are associated with the acquisition, use and storage of iron [*Rocap et al.*, 2003].

[32] Even so, *Mann and Chisholm* [2000] have argued that dissolved iron concentrations of ~0.02 nM were limiting the growth rate of *Prochlorococcus* in the eastern equatorial Pacific. Thus a similar situation, iron limitation of *Prochlorococcus*, may develop in the lower euphotic zone of the Sargasso Sea during late summer. In this regard, it is important to note that algal iron requirements are expected to increase under low irradiance [*Raven*, 1990; *Sunda and Huntsman*, 1997]; that is, growth limitation due to low iron availability is likely to be exacerbated under the low-light conditions in the DCM.

[33] A comparison of the relative concentrations of dissolved iron and macronutrients may provide some indication of the proximate limiting nutrient within the DCM, which coincides with the top of the nitracline. Unfortunately, we are only able to make this comparison for iron and nitrate+nitrite at 150 m depth, since our measurements are close to the analytical detection limits for dissolved inorganic phosphate at 100–150 m depth, and for dissolved nitrate+nitrite at 100 m depth. We assume that the concentrations of dissolved Fe and dissolved nitrate+nitrite represent the major pools of iron and nitrogen, respectively, that are directly available to phytoplankton within the DCM. If we take ~6 μmol/mol as an optimum cellular Fe:C ratio for small phytoplankton [*Moore et al.*, 2004], recognizing that this value is poorly constrained, then we obtain ~40 μmol/mol as an optimum cellular Fe:N ratio, assuming a Redfield C:N ratio. The data from our summer 2003 cruise (Figures 2d and 2e) yield dissolved Fe:nitrate+nitrite ratios of 34–370 μmol/mol at 150 m depth, suggesting that the lowest dissolved Fe concentrations may indeed approach values that are sub-optimal for algal growth. However, this calculation does not provide convincing evidence for iron limitation of low-light *Prochlorococcus* ecotypes, which are able to utilize nitrite but not nitrate [*L. R. Moore et al.*, 2002; *Rocap et al.*, 2003].

[34] Importantly, we note that subsurface minima in dissolved iron have also been reported in the subtropical North Pacific [*Bruland et al.*, 1994; *Boyle et al.*, 2005]; hence such features may be typical of the subtropical gyres during late summer. This leads us to propose that widespread iron limitation may develop in subsurface waters of the subtropical gyres during late summer, where tiny *Prochlorococcus* are often the most abundant autotrophic organism [*Partensky et al.*, 1999].

[35] The relatively low dFe concentrations (0.09–0.26 nM) measured in the upper-ocean samples from the spring 2004 cruise (late April) also suggest that iron availability might regulate the growth of larger phytoplankton in the BATS region during the spring bloom period (January–March), when surface waters contain elevated concentrations of macronutrients and the export of particulate organic matter is relatively high [*Steinberg et al.*, 2001]. If dissolved iron concentrations are this low during the spring bloom period, then iron supply may

significantly impact the assimilation and export of carbon and nutrient elements in the Sargasso Sea. Measurements of iron in the surface mixed layer before and during the spring bloom period (i.e., in winter and early spring) are required to test this hypothesis.

3.6. Concluding Remarks

[36] The results presented in this paper provide strong evidence for the existence of a seasonal iron cycle in surface waters of the Sargasso Sea, as proposed by *Wu and Boyle* [2002]. The seasonal changes in iron concentrations are attributed to the temporal decoupling of sources and sinks of iron in surface waters in this region, whereby eolian iron input (source) dominates during summer and fall, and biological uptake, scavenging, vertical particle export and convective mixing (sinks) dominate during winter and spring. Hence the distribution of iron in surface waters of the Sargasso Sea, and the ecological and biogeochemical consequences of this distribution, should be sensitive to the magnitude of dust inputs in summer, primary production in winter-spring, and convective mixing in winter, all of which are known to vary on interannual and longer-term timescales [*Bates and Hansell*, 2004; *Lomas and Bates*, 2004; *Prospero and Lamb*, 2003]. Further time series observations are required to test this hypothesis.

[37] Our results also provide new boundary conditions for the inclusion of iron in biogeochemical models of the Sargasso Sea, and perhaps other oceanic regions that receive high eolian iron inputs during periods of seasonal stratification. Moreover, our conclusions regarding the effective solubility of aerosol iron, and the potential role of iron in limiting the growth of phytoplankton (particularly *Prochlorococcus*) in subsurface waters, may be broadly applicable to the subtropical gyres. However, our conclusions are based on a very limited data set. Further measurements, both time series and synoptic, are needed to define and understand the range of temporal and spatial variability of iron in the Sargasso Sea, and to evaluate the role of iron in regulating ecological and biogeochemical processes in this oceanic region.

[38] **Acknowledgments.** The authors gratefully acknowledge the captain and crew of RV *Weatherbird II*. We thank Lee Black, Scott Collins, Stuart Halewood, Judy Leonard, Valery Kosnyrev, Keven Neely and Simon Tomko for their contributions to the field program. We are grateful to Robert Leben, Colorado Center for Astrodynamics Research, University of Colorado, for providing the altimetric data, which were essential for targeted sampling of the eddy features described in this study. Comments provided by Rob Sherrell, Ed Sholkovitz and an anonymous reviewer significantly improved the manuscript. Funding for this work was provided by the U.S. National Science Foundation (OCE-0222053 to P. N. S., OCE-0222046 to T. M. C., and OCE-0241310 to D. J. M.), the U.S. National Aeronautics and Space Administration (NAG5-11265 to D. J. M.), the Australian Research Council (DP0342826 to A. R. B.), the Antarctic Climate and Ecosystems Cooperative Research Center, and the H. Unger Vetlesen Foundation. This is BBSR contribution 1663 and WHOI contribution 11352.

References

Archer, D., and K. Johnson (2000), A model of the iron cycle in the ocean, *Global Biogeochem. Cycles*, *14*, 269–279.

Arimoto, R., R. A. Duce, B. J. Ray, W. G. Ellis Jr., J. D. Cullen, and J. T. Merrill (1995), Trace elements in the atmosphere over the North Atlantic, *J. Geophys. Res.*, *100*, 1199–1213.

Arimoto, R., R. A. Duce, B. J. Ray, and U. Tomza (2003), Dry deposition of trace elements to the western North Atlantic, *Global Biogeochem. Cycles*, *17*(1), 1010, doi:10.1029/2001GB001406.

Aumont, O., E. Maier-Reimer, S. Blain, and P. Monfray (2003), An ecosystem model of the global ocean including Fe, Si, P colimitations, *Global Biogeochem. Cycles*, *17*(2), 1060, doi:10.1029/2001GB001745.

Baker, A. R., T. D. Jickells, M. Witt, and K. L. Linge (2005), Trends in the solubility of iron, aluminium, manganese and phosphorus in aerosol collected over the Atlantic Ocean, *Mar. Chem.*, in press.

Bates, N. R., and D. A. Hansell (2004), Temporal variability of excess nitrate in the subtropical mode water of the North Atlantic, *Mar. Chem.*, *84*, 225–241.

Behrenfeld, M., and Z. S. Kolber (1999), Widespread iron limitation of phytoplankton in the south Pacific Ocean, *Science*, *283*, 840–843.

Bell, J., J. Betts, and E. Boyle (2002), MITESS: A Moored in-situ trace element serial sampler for deep-sea moorings, *Deep Sea Res., Part I*, *49*, 2103–2118.

Berman-Frank, I., J. T. Cullen, Y. Shaked, R. M. Sherrell, and P. G. Falkowski (2001), Iron availability, cellular iron quotas, and nitrogen fixation in *Trichodesmium*, *Limnol. Oceanogr.*, *46*, 1249–1260.

Bowie, A. R., P. N. Sedwick, and P. J. Worsfold (2004), Analytical intercomparison between flow injection-chemiluminescence and flow injection-spectrophotometry for the determination of picomolar concentrations of iron in seawater, *Limnol. Oceanogr. Methods*, *2*, 42–54.

Boyd, P. W., et al. (2000), A mesoscale phytoplankton bloom in the polar Southern Ocean stimulated by iron fertilization, *Nature*, *407*, 695–702.

Boyd, P. W., et al. (2004), The decline and fate of an iron-induced subarctic phytoplankton bloom, *Nature*, *428*, 549–553.

Boyle, E. A., S. D. Chapnick, G. T. Shen, and M. P. Bacon (1986), Temporal variability of lead in the western North Atlantic Ocean, *J. Geophys. Res.*, *91*, 8573–8593.

Boyle, E. A., B. A. Bergquist, R. A. Kayser, and N. Mahowald (2005), Iron, manganese, and lead at Hawaii Ocean Time-series station ALOHA: Temporal variability and an intermediate water hydrothermal plume, *Geochim. Cosmochim. Acta*, *69*, 933–952.

Bruland, K. W., K. J. Orians, and J. P. Cowen (1994), Reactive trace metals in the stratified central North Pacific, *Geochim. Cosmochim. Acta*, *58*, 3171–3182.

Chen, Y., and R. L. Siefert (2004), Seasonal and spatial distributions and dry deposition fluxes of atmospheric total and labile iron over the tropical and subtropical North Atlantic Ocean, *J. Geophys. Res.*, *109*, D09305, doi:10.1029/2003JD003958.

Coale, K. H., et al. (1996), A massive phytoplankton bloom induced by ecosystem-scale iron fertilization experiment in the equatorial Pacific Ocean, *Nature*, *383*, 495–501.

Coale, K. H., P. Worsfold, and H. de Baar (1999), Iron age in oceanography, *Eos Trans. AGU*, *80*, 377–382.

Coale, K. H., et al. (2004), Southern Ocean iron enrichment experiment: Carbon cycling in high- and low-Si waters, *Science*, *304*, 408–414.

Conte, M. H., N. Ralph, and E. H. Ross (2001), Seasonal and interannual variability in deep ocean particle fluxes at the Oceanic Flux Program (OFP)/Bermuda Atlantic Time Series (BATS) site in the western Sargasso Sea near Bermuda, *Deep Sea Res., Part II*, *48*, 1471–1505.

Croot, P. L., P. Streu, and A. R. Baker (2004), Short residence time for iron in surface seawater impacted by atmospheric dry deposition from Saharan dust events, *Geophys. Res. Lett.*, *31*, L23S08, doi:10.1029/2004GL020153.

Dickey, T., et al. (2001), Physical and biogeochemical variability from hours to years at the Bermuda Testbed Mooring site: June 1994–March 1998, *Deep Sea Res., Part II*, *48*, 2105–2140.

Doney, S. C., I. Lima, K. Lindsay, J. K. Moore, S. Dutkiewicz, M. A. M. Friedrichs, and R. J. Matear (2001), Marine biogeochemical modeling: Recent advances and future challenges, *Oceanography*, *14*, 93–107.

DuRand, M. D., R. J. Olson, and S. W. Chisholm (2001), Phytoplankton population dynamics at the Bermuda Atlantic Time-series station in the Sargasso Sea, *Deep Sea Res., Part II*, *48*, 1983–2003.

Falkowski, P. G., R. T. Barber, and V. Smetacek (1998), Biogeochemical controls and feedbacks on ocean primary production, *Science*, *281*, 200–206.

Fitzwater, S. E., K. S. Johnson, R. M. Gordon, K. H. Coale, and W. O. Smith (2000), Trace metal concentrations in the Ross Sea and their relationship with nutrients and growth, *Deep Sea Res., Part II*, *47*, 3159–3178.

Fung, I., S. K. Meyn, I. Tegen, S. C. Doney, J. G. John, and J. K. B. Bishop (2000), Iron supply and demand in the upper ocean, *Global Biogeochem. Cycles*, *14*, 281–295.

Gao, Y., S. Fan, and J. L. Sarmiento (2003), Aeolian iron input to the ocean through precipitation scavenging: A modeling perspective and its

implication for natural iron fertilization in the ocean, *J. Geophys. Res.*, *108*(D7), 4221, doi:10.1029/2002JD002420.
Gervais, F., U. Riebesell, and M. Y. Gorbunov (2002), Changes in primary productivity and chlorophyll a in response to iron fertilization in the Southern Polar Frontal Zone, *Limnol. Oceanogr.*, *47*, 1324–1335.
Gordon, R. M., K. H. Coale, and K. S. Johnson (1997), Iron distributions in the equatorial Pacific: Implications for new production, *Limnol. Oceanogr.*, *42*, 419–431.
Hand, J. L., N. M. Mahowald, Y. Chen, R. L. Siefert, C. Luo, A. Subramaniam, and I. Fung (2004), Estimates of atmospheric-processed soluble iron from observations and a global mineral aerosol model: Biogeochemical implications, *J. Geophys. Res.*, *109*, D17205, doi:10.1029/2004JD004574.
Hutchins, D. A., and K. W. Bruland (1998), Iron-limited diatom growth and Si:N uptake ratios in a coastal upwelling regime, *Nature*, *393*, 561–564.
Hutchins, D. A., et al. (2002), Phytoplankton iron limitation in the Humboldt Current and Peru Upwelling, *Limnol. Oceanogr.*, *47*, 997–1011.
Jickells, T. D. (1999), The inputs of dust derived elements to the Sargasso Sea: A synthesis, *Mar. Chem.*, *68*, 5–14.
Jickells, T. D., et al. (2005), Global iron connections between desert dust, ocean biogeochemistry and climate, *Science*, *308*, 67–71.
Johnson, K. S., R. M. Gordon, and K. H. Coale (1997), What controls dissolved iron concentrations in the world ocean?, *Mar. Chem.*, *57*, 137–161.
Johnson, K. S., J. K. Moore, and W. O. Smith (2002), Workshop highlights iron dynamics in ocean carbon cycle, *Eos Trans. AGU*, *83*, 482–484.
Kim, G., and T. M. Church (2001), Seasonal biogeochemical fluxes of ^{234}Th and ^{210}Po in the upper Sargasso Sea: Influence by atmospheric iron deposition, *Global Biogeochem. Cycles*, *15*, 651–661.
Kim, G., and T. M. Church (2002), Wet deposition of trace elements and radon daughter systematics in the South and equatorial Atlantic atmosphere, *Global Biogeochem. Cycles*, *16*(3), 1046, doi:10.1029/2001GB001407.
Kim, G., N. Hussain, and T. M. Church (2003), Tracing the advection of organic carbon into the subsurface Sargasso Sea using a ^{228}Ra/^{226}Ra tracer, *Geophys. Res. Lett.*, *30*(16), 1874, doi:10.1029/2003GL017565.
Leben, R. R., G. H. Born, and B. R. Engebreth (2002), Operational altimeter data processing for mesoscale monitoring, *Mar. Geod.*, *25*, 3–18.
Lomas, M. W., and N. R. Bates (2004), Potential controls on interannual partitioning of organic carbon during the winter/spring phytoplankton bloom at the Bermuda Atlantic time-series study (BATS) site, *Deep Sea Res., Part I*, *51*, 1619–1636.
Mann, E., and S. W. Chisholm (2000), Iron limits the cell division rate of *Prochlorococcus* in the Equatorial Pacific Ocean, *Limnol. Oceanogr.*, *45*, 1067–1076.
Maring, H., D. L. Savoie, M. A. Izaguirre, L. Custals, and J. S. Reid (2003), Mineral dust aerosol size distribution change during atmospheric transport, *J. Geophys. Res.*, *108*(D19), 8592, doi:10.1029/2002JD002536.
Martin, J. H., R. M. Gordon, and S. E. Fitzwater (1990), Iron deficiency limits phytoplankton growth in Antarctic waters, *Global Biogeochem. Cycles*, *4*, 5–12.
Martin, J. H., et al. (1994), Testing the iron hypothesis in ecosystems of the equatorial Pacific Ocean, *Nature*, *371*, 123–129.
Measures, C. I., J. Yuan, and J. A. Resing (1995), Determination of iron in seawater by flow injection analysis using in-line preconcentration and spectrophotometric detection, *Mar. Chem.*, *50*, 1–10.
Michaels, A. F., and A. H. Knap (1996), Overview of the U.S. JGOFS Bermuda Atlantic Time-series Study and the Hydrostation S Program, *Deep Sea Res., Part II*, *43*, 157–198.
Moore, J. K., S. C. Doney, D. M. Glover, and I. Y. Fung (2002), Iron cycling and nutrient-limitation patterns in surface waters of the World Ocean, *Deep Sea Res., Part II*, *49*, 463–507.
Moore, J. K., S. C. Doney, and K. Lindsay (2004), Upper ocean ecosystem dynamics and iron cycling in a global three-dimensional model, *Global Biogeochem. Cycles*, *18*, GB4028, doi:10.1029/2004GB002220.
Moore, L. R., A. F. Post, G. Rocap, and S. W. Chisholm (2002), Utilization of different nitrogen sources by the marine cyanobacteria *Prochlorococcus* and *Synechococcus*, *Limnol. Oceanogr.*, *47*, 989–996.
Olson, R. J., S. W. Chisholm, E. R. Zettler, M. A. Altabet, and J. A. Dusenberry (1990), Spatial and temporal distributions of prochlorophyte picoplankton in the North-Atlantic Ocean, *Deep Sea Res., Part I*, *37*, 1033–1051.
Parekh, P., M. J. Follows, and E. Boyle (2004), Modeling the global ocean iron cycle, *Global Biogeochem. Cycles*, *18*, GB1002, doi:10.1029/2003GB002061.
Partensky, F., W. R. Hess, and D. Vaulot (1999), *Prochlorococcus*, a marine photosynthetic prokaryote of global significance, *Microbiol. Mol. Biol. Rev.*, *63*, 106–127.
Prospero, J. M., and J. P. Lamb (2003), African droughts and dust transport to the Caribbean: Climate change and implications, *Science*, *302*, 1024–1027.
Prospero, J. M., P. Ginoux, O. Torres, S. Nicholson, and T. E. Gill (2002), Environmental characterization of global sources of atmospheric soil dust identified with the NIMBUS 7 Total Ozone Mapping Spectrometer (TOMS) absorbing aerosol product, *Rev. Geophys.*, *40*(1), 1002, doi:10.1029/2000RG000095.
Raven, J. A. (1990), Predictions of Mn and Fe use efficiencies of phototrophic growth as a function of light availability for growth and C assimilation pathway, *New Phytol.*, *116*, 1–17.
Reid, J. S., et al. (2003), Comparison of size and morphological measurements of coarse mode dust particles from Africa, *J. Geophys. Res.*, *108*(D19), 8593, doi:10.1029/2002JD002485.
Rocap, G., et al. (2003), Genome divergence in two *Prochlorococcus* ecotypes reflects oceanic niche differentiation, *Nature*, *424*, 1042–1047.
Rueter, J. G. (1988), Iron stimulation of photosynthesis and nitrogen fixation in *Anabaena* 7120 and *Trichodesmium* (Cyanophyceae), *J. Phycol.*, *24*, 249–254.
Sarthou, G., et al. (2003), Atmospheric iron deposition and sea-surface dissolved iron concentrations in the eastern Atlantic Ocean, *Deep Sea Res., Part I*, *50*, 1339–1352.
Sedwick, P. N., and G. R. DiTullio (1997), Regulation of algal blooms in Antarctic shelf waters by the release of iron from melting sea ice, *Geophys. Res. Lett.*, *24*, 2515–2518.
Sedwick, P. N., P. R. Edwards, D. J. Mackey, F. B. Griffiths, and J. S. Parslow (1997), Iron and manganese in surface waters of the Australian subantarctic region, *Deep Sea Res., Part I*, *44*, 1239–1253.
Sedwick, P. N., G. R. DiTullio, and D. J. Mackey (2000), Iron and manganese in the Ross Sea, Antarctica: Seasonal iron limitation in Antarctic shelf waters, *J. Geophys. Res.*, *105*, 11,321–11,336.
Steinberg, D. K., C. A. Carlson, N. R. Bates, R. J. Johnson, A. F. Michaels, and A. H. Knap (2001), Overview of the US JGOFS Bermuda Atlantic Time-series Study (BATS): A decade-scale look at ocean biology and biogeochemistry, *Deep Sea Res., Part II*, *48*, 1405–1447.
Sunda, W. G., and S. A. Huntsman (1997), Interrelated influence of iron, light and cell size on marine phytoplankton growth, *Nature*, *390*, 389–392.
Ting, C. S., G. Rocap, J. King, and S. W. Chisholm (2002), Cyanobacterial photosynthesis in the oceans: Origins and significance of divergent light-harvesting strategies, *Trends Microbiol.*, *10*, 134–142.
Tsuda, A., et al. (2003), A mesoscale iron enrichment in the western subarctic Pacific induces a large centric diatom bloom, *Science*, *300*, 958–961.
Veron, A. J., and T. M. Church (1997), Use of stable lead isotopes and trace metals to characterize air mass sources into the eastern North Atlantic, *J. Geophys. Res.*, *102*, 2849–2858.
Weber, L., C. Völker, M. Schartau, and D. A. Wolf-Gladrow (2005), Modeling the speciation and biogeochemistry of iron at the Bermuda Atlantic Time-series Study site, *Global Biogeochem. Cycles*, *19*, GB1019, doi:10.1029/2004GB002340.
Wu, J., and E. Boyle (2002), Iron in the Sargasso Sea: Implications for the processes controlling dissolved Fe distribution in the ocean, *Global Biogeochem. Cycles*, *16*(4), 1086, doi:10.1029/2001GB001453.
Wu, J., and G. W. Luther III (1996), Spatial and temporal distribution of iron in the surface water of the northwestern Atlantic Ocean, *Geochim. Cosmochim. Acta*, *60*, 2729–2741.
Zhu, X. R., J. M. Prospero, and F. J. Millero (1997), Diel variability of soluble Fe (II) and soluble total Fe in North African dust in the trade winds at Barbados, *J. Geophys. Res.*, *102*(D17), 21,297–21,306.

K. M. Achilles, University of California, Santa Cruz, Santa Cruz, California, USA.
A. R. Bowie, University of Tasmania, Hobart, Tasmania, Australia.
T. M. Church and M. M. Sarin, University of Delaware, Newark, Delaware, USA.
R. J. Johnson, C. M. Marsay, and P. N. Sedwick, Bermuda Biological Station for Research, Ferry Reach, St. George's, GE01 Bermuda. (psedwick@bbsr.edu)
P. J. Lethaby, University of Hawaii, Honolulu, Hawaii, USA.
D. J. McGillicuddy, Woods Hole Oceanographic Institution, Woods Hole, Massachusetts, USA.
S. J. Ussher, University of Plymouth, Plymouth, UK.

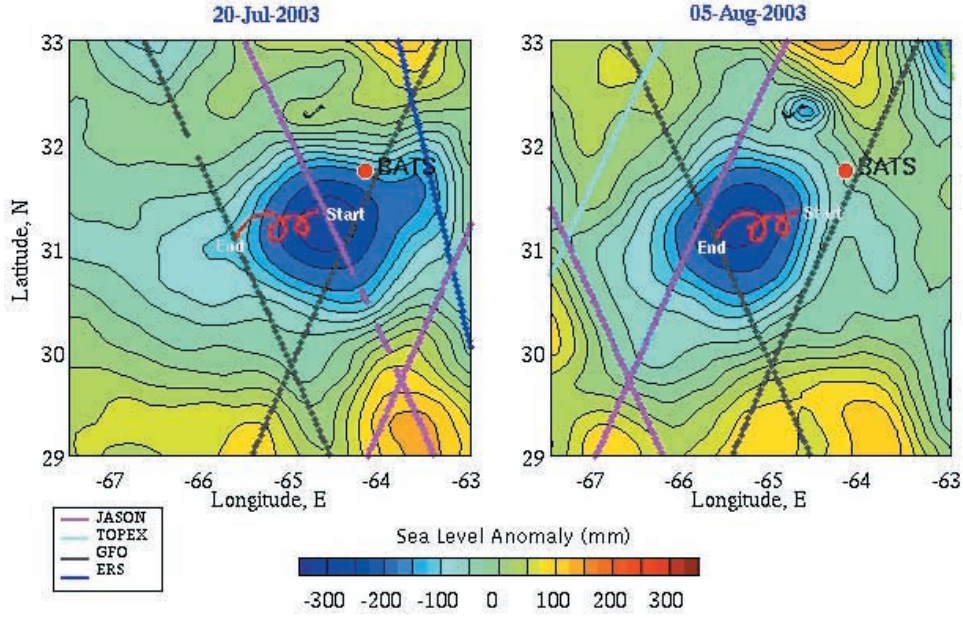

Figure 1. Objective analysis of sea level anomaly for (left) 20 July 2003 (just prior to summer 2003 cruise) and (right) 5 August 2003 (near end of summer 2003 cruise), showing location of target eddy (negative sea level anomaly shown in blue) and BATS site. The track of the drifting array during the cruise (red) is overlain on both panels, with initial (start) and final (end) points indicated. Real-time altimetric data were obtained from http://www-ccar.colorado.edu/~realtime/nwatlantic-real-time_ssh; altimeter ground tracks used in the analysis are identified in the legend.

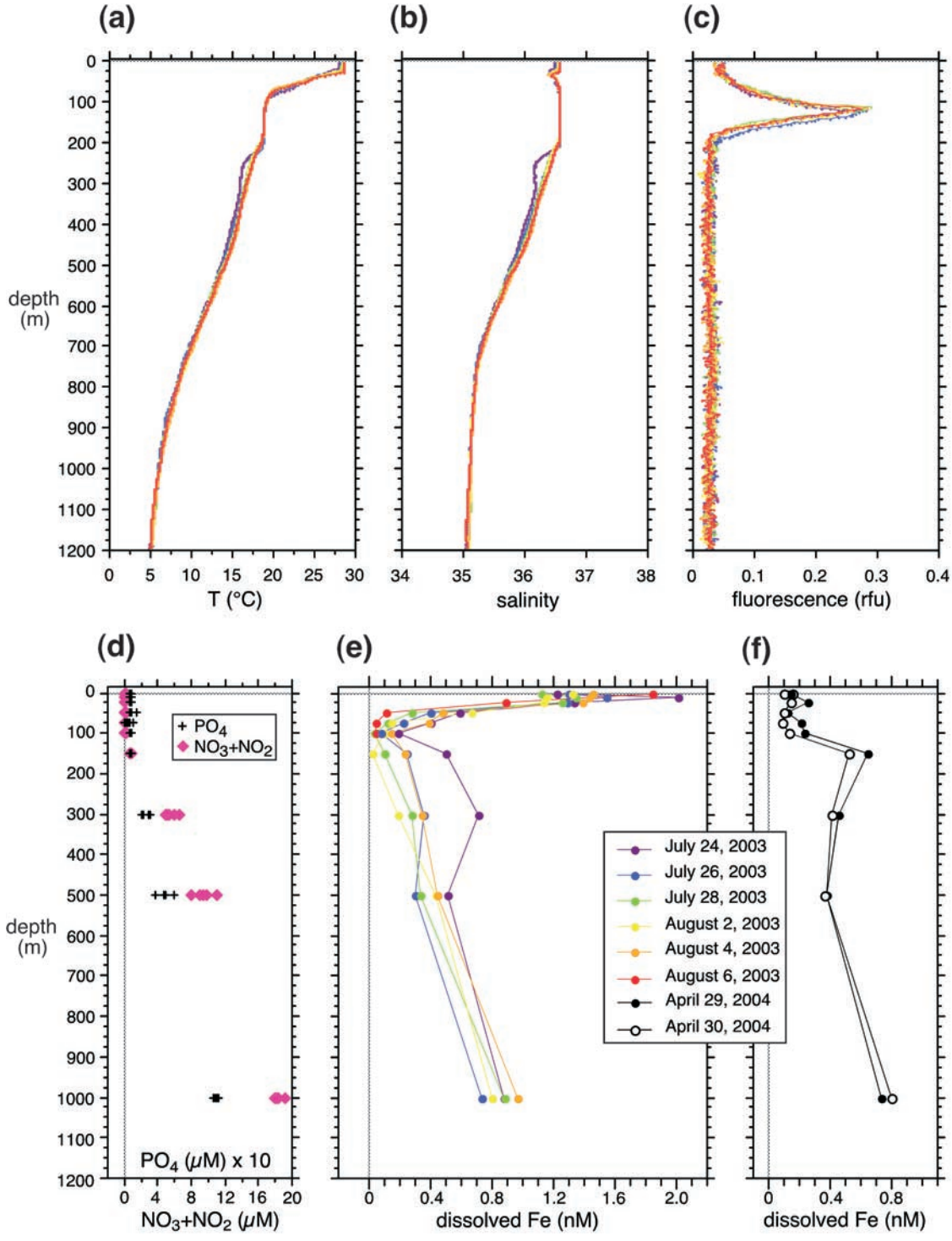

Figure 2. Water column profiles of (a) temperature, (b) salinity, (c) fluorescence, (d) dissolved nitrate+nitite (NO_3 + NO_2) and dissolved inorganic phosphate (PO_4), and (e) dissolved iron during the summer 2003 cruise; and (f) dissolved iron during the spring 2004 cruise. The color of data points in Figures 2a, 2b and 2c correspond to the legend in Figure 2e.